A Highly Stable Eu−MOF Multifunctional Luminescent Sensor for the Effective Detection of Fe^{3+}, $Cr_2O_7^{2-}$/CrO_4^{2-} and Aspartic Acid in Aqueous Systems

Yin−Xia Sun*, Geng Guo, Wen−Min Ding, Wen−Yu Han, Juan Li, Zhe−Peng Deng

(School of Chemical and Chemical Engineering, Lanzhou Jiaotong University, Lanzhou 730070, China)

Synthesis of 4,4',4''−triazine−2,4,6−tribenzoic acid (H_3L). The ligand **H_3L** was prepared by the method reported in literature.[1] The synthesis process is shown in **Scheme S1**. 4-cyano-toluene (1.50 g, 12.80 mmol) was slowly dropwise to trifluoromethanesulfonic acid (3.0 mL) and stirred at room temperature for 24 hours. After the reaction is completed, the reaction mixture is poured into the ice water mixture, and then neutralized with ammonia to obtain white precipitation. Filter the obtained sediment, collect the filter cake, and finally rinse with water and acetone. Use toluene recrystallization. Yield: 74.2%. ^{1}H-NMR (500 MHz, $CDCl_3$): δ = 8.65 ppm (d, J = 10 Hz, 6H), 7.36(d, J = 10 Hz, 6H), 2.47 (s, 9H) (Figure S1).

The intermediate 2,4,6-tris(4-methylphenyl)-1,3,5-triazine (1.00 g, 2.80 mmol) was dissolved in a mixed solution containing acetic acid (60.0 mL, 1.00 mol) and sulfuric acid (2.0 mL, 37.50 mmol). Dissolve crystalline chromium trioxide (2.62 g, 26.20 mmol) and acetic anhydride (6.6 mL, 70.50 mmol) and add them to the above mixed solution. Under the condition of simultaneous stirring at a temperature lower than 50 °C, stir the green slurry for 12 hours and place it overnight. The reactants were poured into ice water, and the resulting solution was fully mixed and filtered. The collected solids were washed with water and dissolved in 200.0 mL 2.0 mol·L^{-1} NaOH solution and the insoluble solids were removed by filtration. The filtrate was acidified with 6.0 mol·L^{-1} HCl solution and filtered to obtain cream color precipitation. The solid was obtained by recrystallization with H_2O. Yield: 54.7%. ^{1}H-NMR (500 MHz, DMSO-d$_6$): δ 13.37 (s, 3H), 8.84 (d, J = 10 Hz, 6H), 8.20 (d, J = 10 Hz, 6H) (Figure S2).

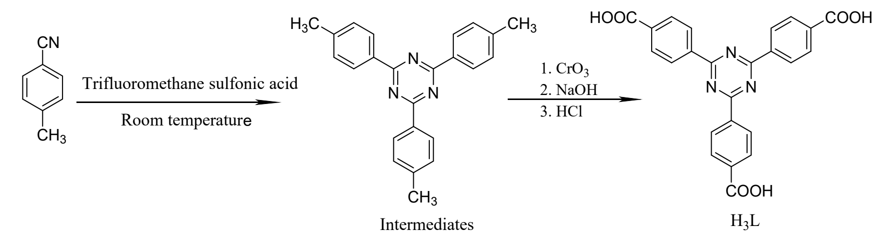

Scheme S1 Synthetic routes of 4,4',4''−triazine−2,4,6−tribenzoic acid.

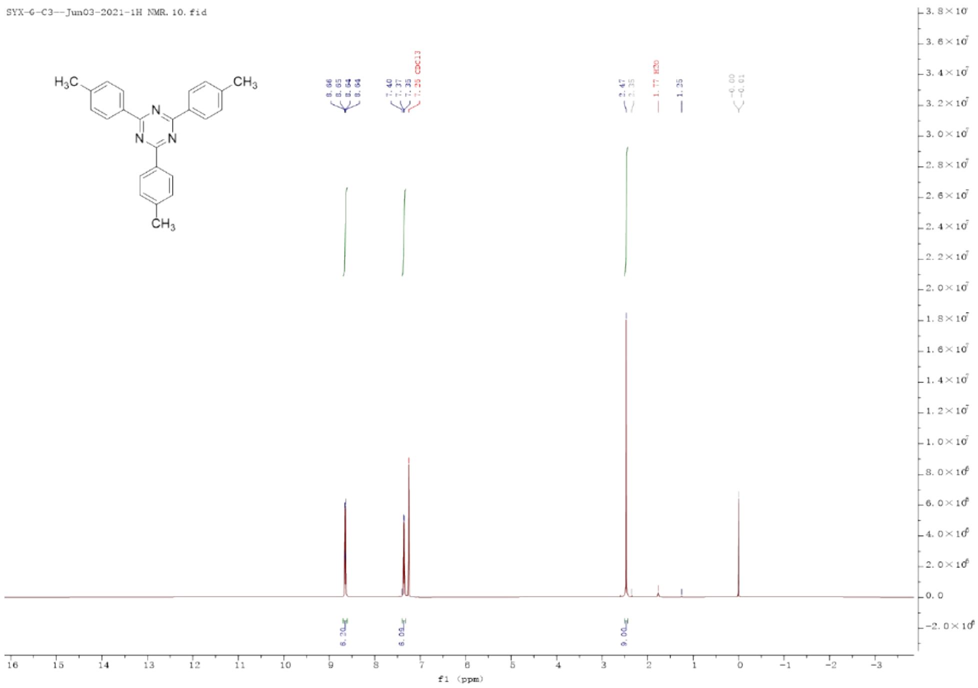

Fig. S1 ^{1}H NMR spectra of 2,4,6-tris(4-methylphenyl)-1,3,5-triazine.

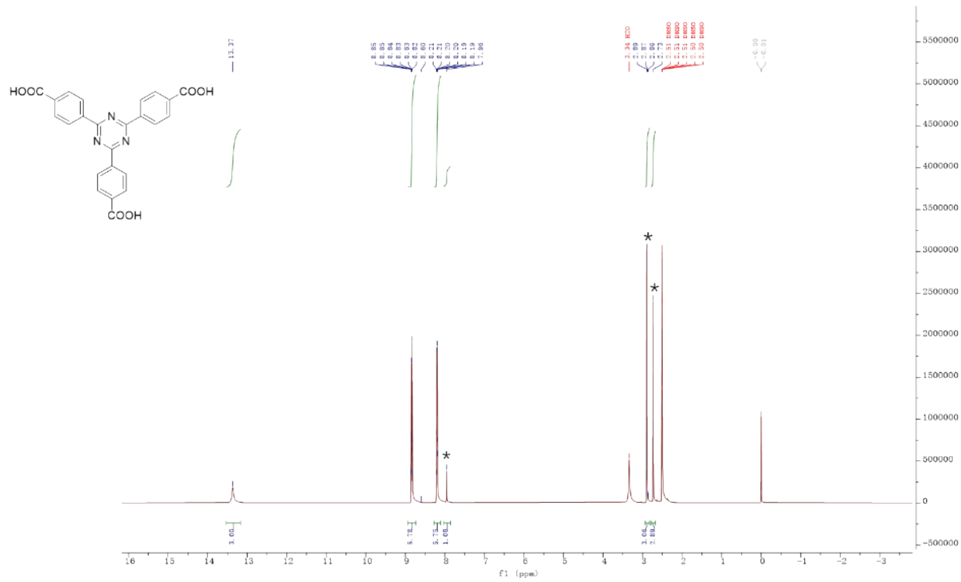

Fig. S2 ^{1}H NMR spectra of 4,4',4''−triazine−2,4,6−tribenzoic acid.

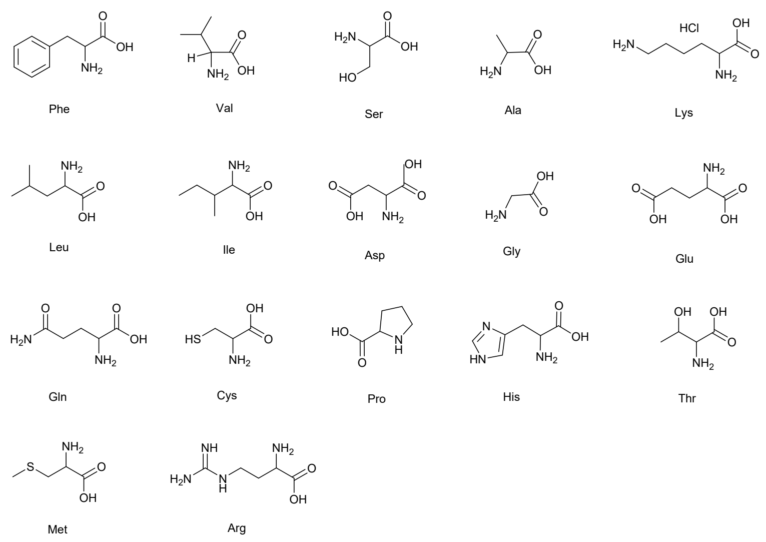

Fig. S3 Structural formula for partial amino acids used for fluorescence sensing

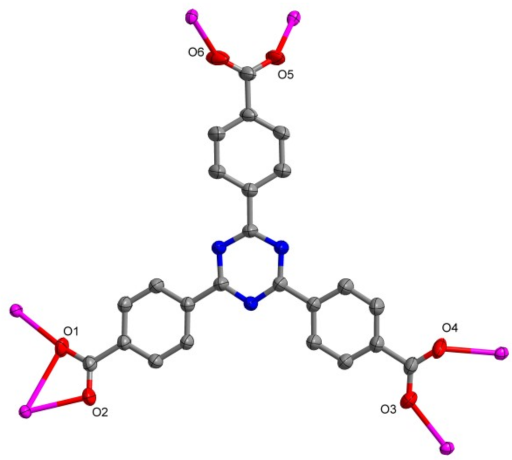

Fig. S4 The connection mode of ligand H_3L with Eu^{3+} μ_6-κ^7,O1,O1,O2,O3,O4,O5,O6.

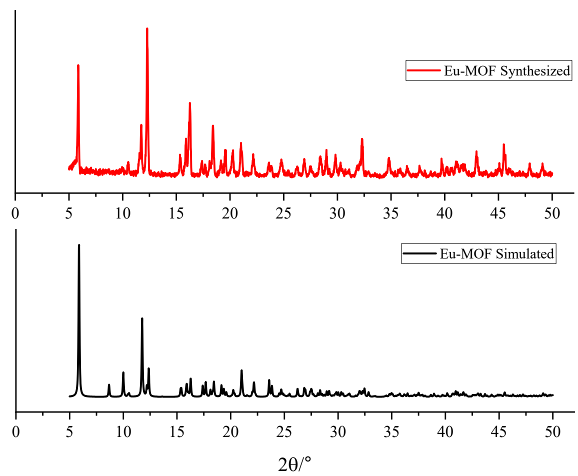

Fig. S5 PXRD of **Eu-MOF**.

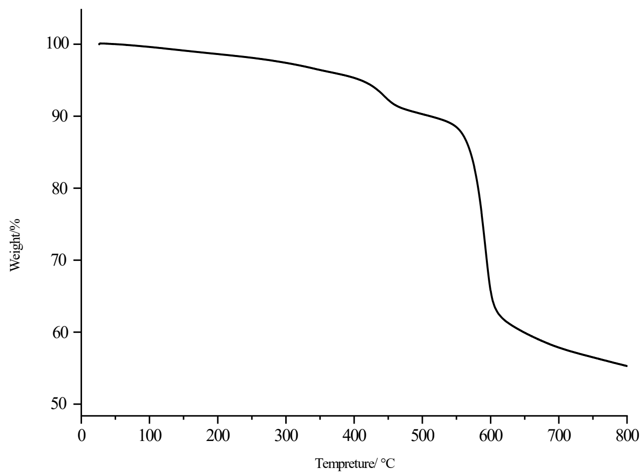

Fig. S6 TGA curve of **Eu-MOF**.

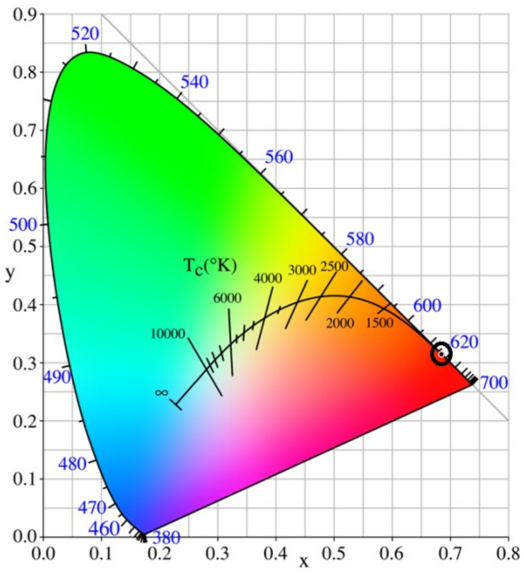

Fig. S7 CIE coordinates of **Eu-MOF**.

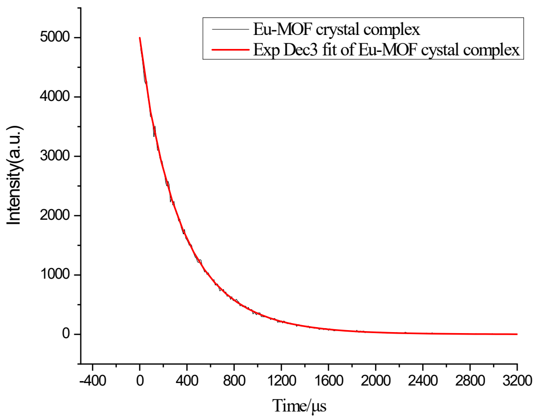

Fig. S8 Fluorescence lifetime of **Eu-MOF**.

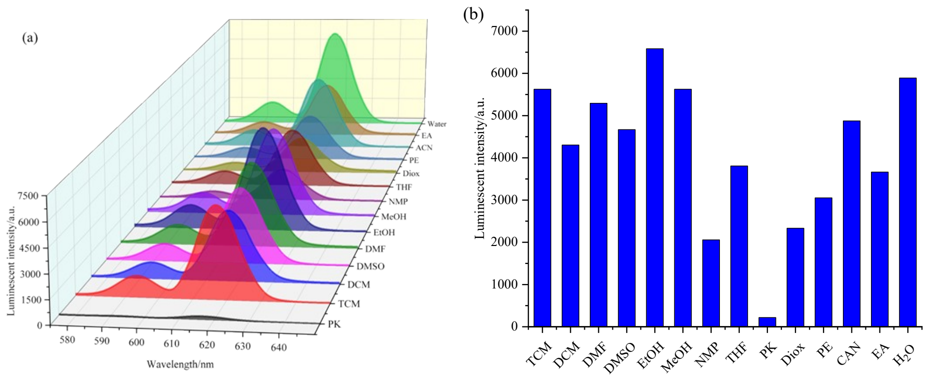

Fig. S9 (a) Luminescent spectra of **Eu−MOF** in different solvents; (b) Histogram of relative luminescent intensity of **Eu-MOF** at 618 nm

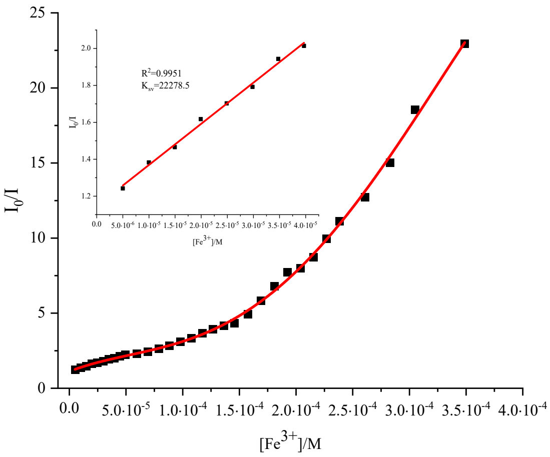

Fig. S10 S−V plot of **Eu-MOF** upon different concentrations of Fe^{3+} ions (inset: the linearity relationship of luminescent quenching at low concentration).

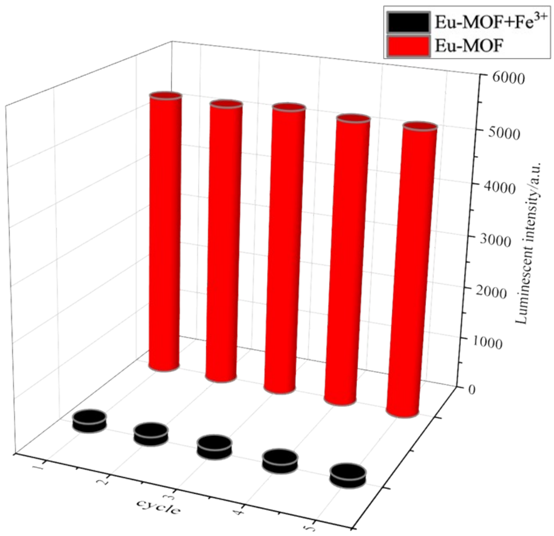

Fig. S11 Relative intensities of the $^5D_0 \rightarrow {}^7F_2$ transitions (616 nm) for the **Eu-MOF** reused for several cycles in Fe^{3+}.

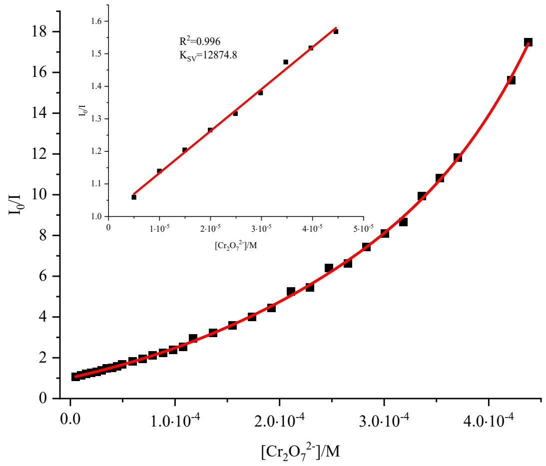

Fig. S12 S−V plot of Eu-MOF upon different concentrations of $Cr_2O_7^{2-}$ ions (inset: the linearity relationship of luminescent quenching at low concentration).

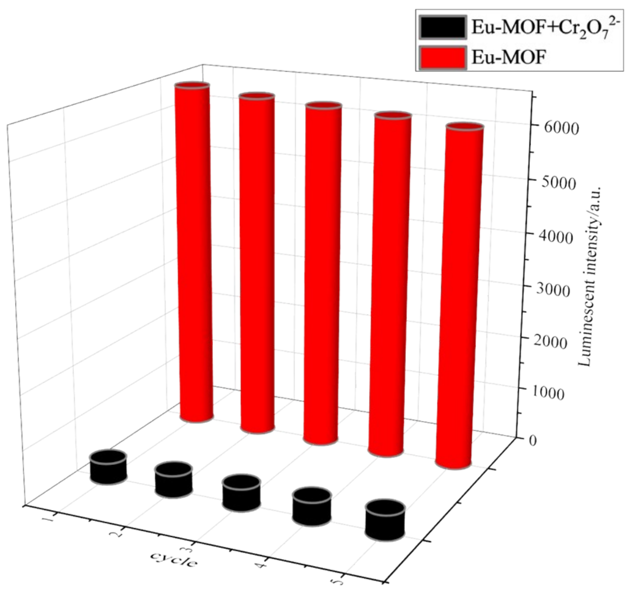

Fig. S13 Relative intensities of the $^5D_0 \rightarrow {}^7F_2$ transitions (616 nm) for the **Eu-MOF** reused for several cycles in $Cr_2O_7^{2-}$.

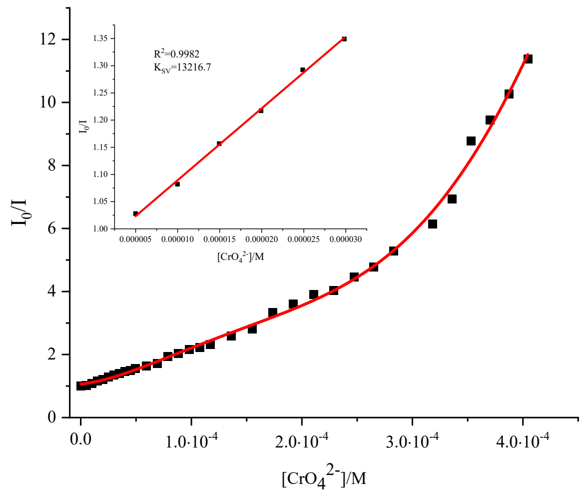

Fig. S14 S−V plot of **Eu-MOF** upon different concentrations of CrO_4^{2-} ions (inset: the linearity relationship of luminescent quenching at low concentration.

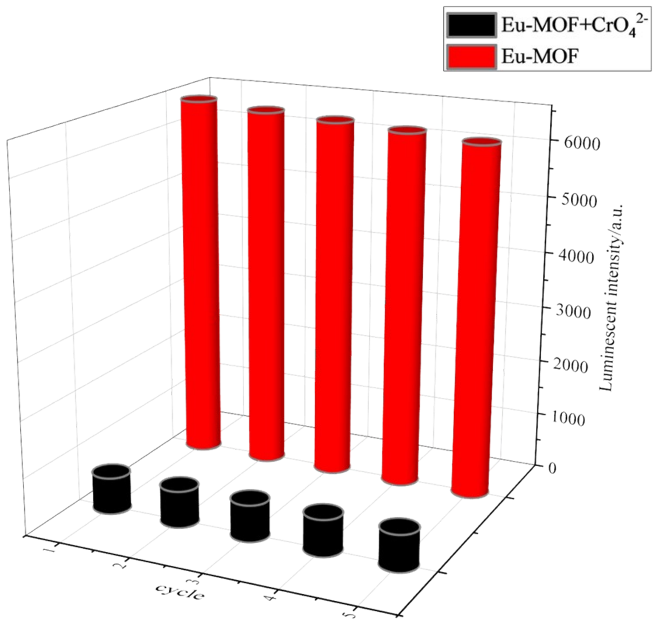

Fig. S15 Relative intensities of the $^5D_0 \rightarrow {}^7F_2$ transitions (616 nm) for the **Eu-MOF** reused for several cycles in CrO_4^{2-}.

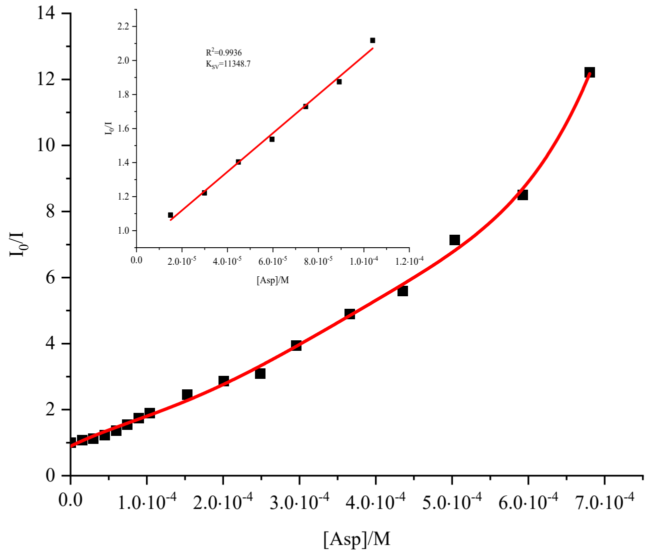

Fig. S16 S−V plot of **Eu-MOF** upon different concentrations of Asp ions (inset: the linearity relationship of luminescent quenching at low concentration).

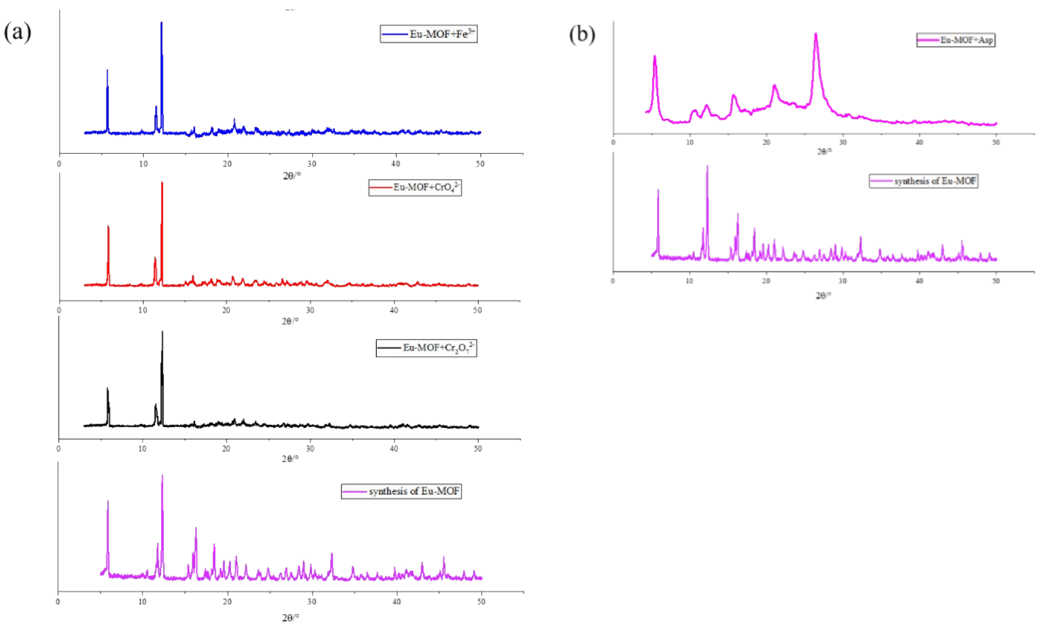

Fig. S17 PXRD of **Eu-MOF** after Fe^{3+}, CrO_4^{2-}, $Cr_2O_7^{2-}$ and Asp treatment.

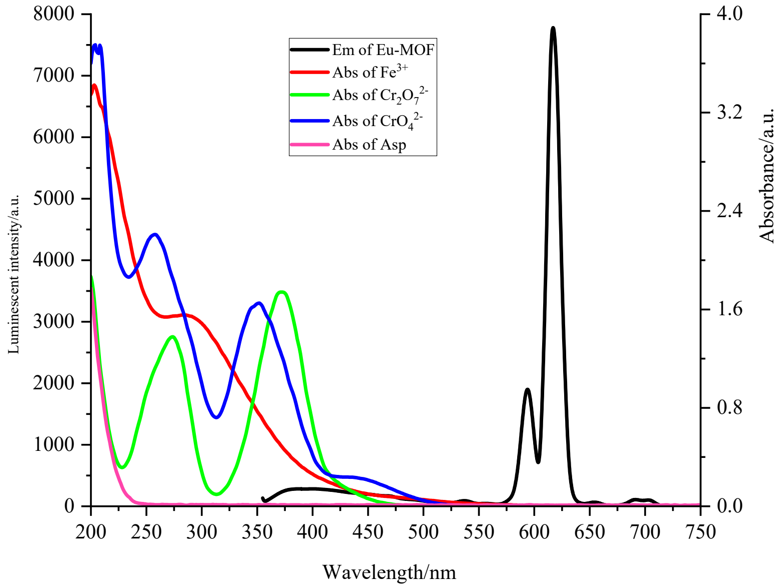

Fig. S18 Luminescent emission spectra of **Eu−MOF** and absorption spectra of Fe^{3+}, $Cr_2O_7^{2-}$, CrO_4^{2-} and Asp in water.

Table S1 Crystallographic data and structure refinement for **Eu-MOF**

Identification code	**Eu-MOF**
Empirical formula	$C_{408}H_{248}Eu_{16}N_{52}O_{112}$
Formula weight	10101.93
Temperature/K	292.4(3)
Crystal system	orthorhombic
Space group	*Fddd*
a/Å	22.3041(9)
b/Å	28.6028(14)
c/Å	29.0127(13)
α/°	90
β/°	90
γ/°	90
Volume/Å^3	18509.0(15)
Z	2
ρ_{calc} g/cm^3	1.813
μ/mm^{-1}	19.881
F(000)	9928.0
Crystal size/mm^3	0.05 × 0.03 × 0.02
Radiation	CuKα(λ = 1.54184)
2Θ range for data collection/°	10.004 to 139.682
Index ranges	$-27 \leq h \leq 13$, $-34 \leq k \leq 34$, $-34 \leq l \leq 34$
Reflections collected	12214
Independent reflections	4237 [R_{int} = 0.0386, R_{sigma} = 0.0427]
Data/restraints/parameters	4237/546/333
Goodness-of-fit on F^2	1.051
Final R indexes [I>=2σ (I)]	R_1 = 0.0401, wR_2 = 0.0900
Final R indexes [all data]	R_1 = 0.0478, wR_2 = 0.0946
Largest diff. peak/hole / eÅ^{-3}	0.93/-0.90

Table S2. Selected bond lengths [Å] for **Eu–MOF**

Atom	Atom	Length/Å	Atom	Atom	Length/Å
Eu	Eu#	4.0557(6)	Eu	O(1)	2.778(4)
Eu	O(7)	2.425(6)	Eu	O(1)#	2.370(4)
Eu	O(5)B	2.299(4)	Eu	O(3)A	2.334(4)
Eu	O(2)	2.401(4)	Eu	O(4)A#	2.331(4)
Eu	O(6)C	2.337(4)			

#:1-X,1.5-Y,0.5-Z; A:-0.25+X,1-Y,-0.25+Z; A#:1.25-X,0.5+Y,0.75-Z;B:0.75-X,1.25-Y,-0.5+Z; C:0.5+X,1.25-Y,0.75-Z.

Table S3. Selected angles [°] for **Eu–MOF**

Atom	Atom	Atom	Angle/°	Atom	Atom	Atom	Angle/°
O(7)	Eu	O(1)	112.78(19)	O(1)#	Eu	O(7)	146.8(2)
O(5)B	Eu	O(7)	78.5(2)	O(1)#	Eu	O(2)	125.68(15)
O(5)B	Eu	O(2)	151.94(17)	O(1)#	Eu	O(1)	76.33(13)
O(5)B	Eu	O(6)C	83.41(15)	O(3)A	Eu	O(7)	77.7(2)
O(5)B	Eu	O(1)#	79.28(15)	O(3)A	Eu	O(2)	86.36(17)
O(5)B	Eu	O(1)	148.25(13)	O(3)A	Eu	O(6)C	149.97(18)
O(5)B	Eu	O(3)A	87.64(16)	O(3)A	Eu	O(1)#	77.09(16)
O(5)B	Eu	O(4)A#	117.59(18)	O(3)A	Eu	O(1)	67.37(15)
O(2)	Eu	O(7)	73.5(2)	O(4)A#	Eu	O(7)	141.1(2)
O(2)	Eu	O(1)	49.71(13)	O(4)A#	Eu	O(2)	85.49(18)
O(6)C	Eu	O(7)	72.5(2)	O(4)A#	Eu	O(6)C	74.60(17)
O(6)C	Eu	O(2)	88.22(16)	O(4)A#	Eu	O(1)	73.17(16)
O(6)C	Eu	O(1)	127.94(14)	O(4)A#	Eu	O(1)#	71.69(16)
O(6)C	Eu	O(1)#	128.62(18)	O(4)A#	Eu	O(3)A	134.18(16)

#:1-X,1.5-Y,0.5-Z; A:-0.25+X,1-Y,-0.25+Z; A#:1.25-X,0.5+Y,0.75-Z;B:0.75-X,1.25-Y,-0.5+Z; C:0.5+X,1.25-Y,0.75-Z.

Table S4. Comparison of Fe^{3+}, $Cr_2O_7^{2-}$/CrO_4^{2-}, Asp sensing based on MOF-based fluorescent probe.

Compound	Solvents	Substrate	K_{SV}/M	LOD/μM	Ref.
$[Eu_3(bcbp)_3(NO_3)_7]$	DMF	$Cr_2O_7^{2-}$	1.40×10^4	5.6	2
$\{(Me_2NH_2)[Ln_3(PTTBA)_2]\cdot 4DM\cdot 3H_2O\}_n$	H_2O	Fe^{3+}	4.75×10^4	6.32	3
La(III)-TCPE	THF	Fe^{3+}	1.09×10^5	1.69	4
NU-1000	H_2O	$Cr_2O_7^{2-}$	1.34×10^4	1.8	5
$\{Ln(cpon)(Hcpon)(H_2O)_3\}_n$	H_2O	$Cr_2O_7^{2-}$	4.11×10^4	0.25	6
Eu-MOF	H_2O	Fe^{3+}	2.03×10^4	/	7
	H_2O	CrO_4^{2-}	1.92×10^4	/	
	H_2O	$Cr_2O_7^{2-}$	1.14×10^4	/	
Tb-MOF	H_2O	Fe^{3+}	1.20×10^4	/	
	H_2O	CrO_4^{2-}	1.14×10^4	/	
	H_2O	$Cr_2O_7^{2-}$	8.23×10^3	/	
$\{[Cd_{2(}dpc)(bib)(H_2O)]\cdot H_2O\}_n$	H_2O	Asp	/	/	8
Cu/Tb@Zn-MOF	H_2O	Asp	1.33×10^5	4.13	9
CDs-Cu^{2+}	H_2O (pH=4.0)	Asp	/	0.12	10
$\{[Cd(L)(BPDC)]\cdot 2H_2O\}_n$	H_2O	Fe^{3+}	3.63×10^4	2.21	11
	H_2O	$Cr_2O_7^{2-}$	6.4×10^3	37.6	
$\{[Cd(L)(SDBA)(H_2O)]\cdot 0.5H_2O\}_n$	H_2O	Fe^{3+}	3.59×10^4	7.14	
	H_2O	$Cr_2O_7^{2-}$	4.97×10^3	48.6	
Bi-MOF	H_2O/DMF=4:1	Fe^{3+}	2.02×10^4	1.59	12
	H_2O/DMF=4:1	$Cr_2O_7^{2-}$	1.95×10^4	1.64	
(Zn_3-ttb-bdc)	H_2O	Fe^{3+}	5.01×10^4	0.13	13
	H_2O	$Cr_2O_7^{2-}$	6.67×10^4	0.10	
Eu^{3+}@$\{[Ni_2(odip)(H_2O)_4(DMF)]$	DMF/H_2O=2:1	Asp	1.56×10^3	2.51	14
$[Eu\text{-}(L)(H_2O)_2]\cdot DMF\}_n$	H_2O	Asp	1.09×10^3	/	15
Tb-MOF	H_2O	Fe^{3+}	1.28×10^4	0.50	16
	H_2O	$Cr_2O_7^{2-}$	0.84×10^4	2.92	
Eu-MOF	H_2O	Fe^{3+}	2.22×10^4	1.12	*This work*
	H_2O	$Cr_2O_7^{2-}$	1.29×10^4	1.95	
	H_2O	CrO_4^{2-}	1.32×10^4	1.89	
	H_2O	Asp	1.32×10^4	2.20	

REFERENCES

1 J. P. Leite, D. Rodrigues, S. Ferreira, F. Figueira, F. A. A. Paz and G. Gales, *Cryst. Growth Des.*, 2019, **19(3)**, 1610–1615.

2 Z. Y. Li, W. Y. Cai, X. M. Yang, A. L. Zhou, Y. Zhu, H. Wang, X. Zhou, K. C. Xiong, Q. F. Zhang and Y. L. Gai, *Cryst. Growth Des.*, 2020, **20(5)**, 3466–3473.

3 H. T. Chen, L. M. Fan, H. X. Lv and X. T. Zhang, *Inorg. Chem.*, 2020, **59(18)**, 13407–13415.

4 L. Yang, Y. Dou, L. Qin, L. L. Chen, M. Z. Xu, C. Kong, D. P. Zhang, Z. Zhou and S. N. Wang, *Inorg. Chem.*, 2020, **59(22)**, 16644–16653.

5 Z. J. Lin, H. Q. Zheng, H. Y. Zheng, L. P. Lin, Q. Xin and R. Cao, *Inorg. Chem.*, 2017, **56(22)**, 14178–14188.

6 W. Chen, R. Q. Fan, J. Z. Fan, H. Y. Liu, T. C. Sun and P. Wang, *Inorg. Chem.*, 2019, **58(22)**, 15118–15125.

7 H. H. Yu, M. Y. Fan, Q. Liu, Z. M. Su, X. Li, Q. Q. Pan and X. L. Hu, *Inorg. Chem.*, 2020, **59(3)**, 2005–2010.

8 Y. Du, H. Y. Yang, C. Y. Shao, J. W. Liu, Y. T. Yan, L. X. Yu, D. Q. Zhu, C. N. Huang and L. R. Yang, *J. Solid State Chem.*, 2019, **277**, 564-574.

9 G. F. Ji, T. X. Zheng, X. C. Gao and Z. L. Liu, *Sens. Actuators, B*, 2019, **284**, 91–95.

10 S. Karami, M. Shamsipur, A. Barati, *Anal. Chim. Acta*, 2021, **1144**, 26-33.

11 S. G. Chen, Z. Z. Shi, L. Qin, H. L. Jia and H. G. Zheng, *Cryst. Growth Des.*, 2017, **17(1)**, 67–72.

12 Y. Sun, N. Zhang, Q. L. Guan, C. H. Liu, B. Li, Y. K. Zhang, G. H. Li, Y. H. Xing, F. Y. Bai and L. X. Sun, *Cryst. Growth Des.*, 2019, **19(12)**, 7217-7229.

13 S. Gai, R. Q. Fan, J. Zhang, J. K. Sun, P. X. Li, Z. Q. Geng, X. Jiang, Y. Y. Dong, J. Q. Wang and Yulin Yang, *Inorg. Chem.*, 2021, **60**, 10387−10397.

14 Y. Liu, Y. K. Lu, B. Zhang, L. Hou and Y. Y. Wang, *Inorg. Chem.*, 2020, **59(11)**, 7531–7538.

15 A. F. Yang, S. L. Hou, Y. Shi, G. L. Yang, D. B. Qin and B. Zhao, *Inorg. Chem.*, 2019, **58(9)**, 6356–6362.

16 J. X. Li , B. Q. Yu , L. H. Fan , L. Wang , Y. C. Zhao , C. Y. Sun, W. J. Li and Z. D. Chang, *J. Solid State Chem.*, 2022, **306**, 122782.